Journal of Magnetic Resonance Open 12–13 (2022) 100084

Contents lists available at ScienceDirect

Journal of Magnetic Resonance Open

journal homepage: www.sciencedirect.com/journal/journal-of-magnetic-resonance-open

Research Article

Mechanically oscillating sample under magnetic field gradients: MOS-NMR

Everton Lucas-Oliveira [a,*], Agide Gimenez Marassi [a], Arthur Gustavo Araújo-Ferreira [a], Edson Luiz Géa Vidoto [a], Aparecido Donizeti Fernandes de Amorim [a], Willian Andrighetto Trevizan [b], Tito José Bonagamba [a]

[a] São Carlos Institute of Physics, University of São Paulo, PO Box 369, 13560-970, São Carlos, SP, Brazil
[b] Leopoldo Américo Miguez de Mello Research and Development Center – CENPES/Petrobras, Brazil

ARTICLE INFO

Keywords:
NMR well logging
Logging while drilling (LWD)
Mechanically oscillating sample
Porous media
CPMG

ABSTRACT

Nuclear Magnetic Resonance (NMR) has been widely used in Petroleum Science and Engineering to study geological formations (porous media) in laboratories or under well-logging conditions. In both cases, NMR is still evolving to provide more accurate data on well productivity. In well-logging, NMR is one of the main tools used in determining the economic viability of an oil well due to the reliability of measurements of fluid types, porosity, pore size, and permeability of the reservoir under analysis. There are two kinds of NMR well-logging techniques: Wireline and Logging While Drilling (LWD). In the latter, due to the drilling process, measurements are made with the NMR tool translating, vibrating and, in some cases, rotating relatively to the geological formation. To understand the behavior of NMR signals measured under LWD conditions, not yet including displacement and drill vibration, we have recently developed a single-sided magnet, probes, and a mechanical system that emulates a relative sinusoidal motion between the sample and the applied magnetic field. This equipment was used to emulate a LWD tool operating under normal pressure and temperature conditions.

1. Introduction

NMR is a very versatile technique applied to the study of materials in the liquid and solid state [1]. For the oil industry, NMR is present in different stages of the production process, making it essential from well-logging to the analysis of refined products from petroleum [2, 3]. In well-logging, NMR techniques are used to obtain information about the fluids and the porous medium near the well [4–7]. However, information can be obtained in two different ways: after drilling, using a cable NMR tool, known as Wireline Logging, or during drilling, known as Logging While Drilling (LWD) [7–9].

Wireline Logging allows the NMR tool to be kept static while measuring it in a specific region of the well, allowing for longer measurements and advanced techniques. However, these analyses are expensive and economic feasibility must always be considered. On the other hand, LWD occurs concomitantly with the drilling of the well [9], making it supposedly faster and cheaper. Therefore, it aims to extract as much information as possible, ensuring its quality. Significant work has been done in this direction, allowing the use of the NMR technique worldwide by different companies and many efforts have been made to improve the LWD method [10–14].

A recent study published by Coman et al. [10] discusses the Lateral-Motion during the LWD and the respective effects on the NMR signal. The authors considered the most complex case based on LWD results and simulated data, suggesting a formula to describe the lateral-motion flow effect method.

More recently, two studies involving sample motion during NMR measurement have been published, one based on a simulation model [11], and another with experimental results focused on measuring the sample velocity through the accumulate phase [12].

Here, to understand the behavior of NMR signals measured from samples under LWD conditions, we have developed a single-sided magnet [15], probes, and a mechanical system that emulates a relative sinusoidal motion between the sample and the applied magnetic field, Fig. 1. The results show that even in the simplest condition (one-dimensional sinusoidal motion), depending on the frequency and amplitude of the movement, the NMR signal has a behavior that a simple sinusoidal equation cannot describe. Furthermore, controlling the amplitude and the relative position between the sample position and the single-sided magnet, the influence of the lateral movement and the spatial selectivity of the RF pulse are clearly understood.

* Corresponding author.
E-mail address: everton.lucas.oliveira@usp.br (E. Lucas-Oliveira).

https://doi.org/10.1016/j.jmro.2022.100084

Available online 17 November 2022

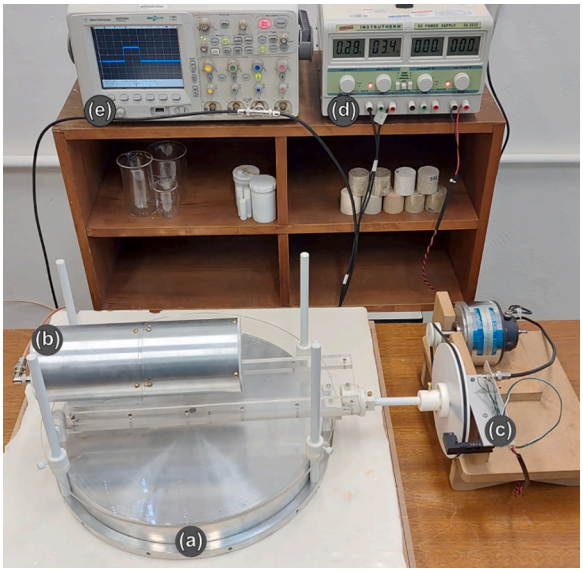

Fig. 1. Experimental setup for MOS-NMR experiments. It consists of: **(a)** single-sided magnet, **(b)** shielded solenoid coil - NMR probe, **(c)** set of pulleys connected to an electric motor powered by a **(d)** DC power supply to control the probe oscillating motion, and an **(e)** oscilloscope to measure the oscillation frequency. Associated with the set of pulleys, there is an optic sensor to synchronize the oscillating motion to the CPMG experiment.

2. Material and methods

2.1. Single-sided NMR tool and sample motion system

This section provides an understanding of the experimental approach for the Mechanically Oscillating Sample (MOS-NMR) simulation under laboratory environment conditions. Although conventional NMR systems generally consist of a high, homogenous magnetic field, a limitation arises from the small functional region for the sample position inside the magnet bore, restricting the maximum dimensions of samples.

To overcome the difficulties mentioned above, the development single-sided magnets and specialized NMR instrumentation by petroleum industries represented an enormous advance in investigating practicable regions for oil exploration [16]. Thus, to mimic the oscillatory motion produced by well logging-while-drilling situation, an experimental setup to simulate this aspect of the experimental procedure was designed, as shown in Fig. 1.

The main and outstanding feature of this equipment is its single-sided magnet. It produces a magnetic field of 470 Gauss and a constant magnetic field gradient of 35.7 Gauss/cm within its sweet spot, which is located at 11 cm from its surface and has both a diameter and a length of 4 cm. The magnet geometry was designed to allow multiple applications, not only limited to the oil industry, but extending, for example, to the healthcare and cement industry, taking into account the large distance between the magnet surface and its sweet spot. The specification of the magnetic gradient field was determined in partnership with the Brazilian oil company - Petrobras. More details about this extremely versatile single-sided magnet can be found in Oliveira-Silva [15].

The NMR probe was developed and built up for the measurements using the single-sided magnet, operating at the ^1H Larmor frequency of 2 MHz. The geometry chosen was a solenoid coil, with 34 turns of AWG 19 enameled copper wire around a PVC support, a diameter of 45 mm, and a length of 50 mm, which can accommodate a cylindrical sample holder with a maximum diameter of 38 mm.

The RF circuit has a conventional construction [17], in which a parallel variable capacitor adjusts the resonance frequency, and a series fixed capacitor adjusts the 50 ohm matching. The probe was designed to have a low-quality factor ($Q \approx 10$) to reduce the ringing time and enable shorter RF pulses. The resistive Q damping was constructed with the association of a non-magnetic, non-inductive set of resistors. The probe was assembled inside a 100 mm diameter and 1.5 mm thick wall cylindrical shaped aluminum structure.

In order to simulate the oscillating motion in an LWD pattern, the probe was fixed on an acrylic table. This table sits on a platform whose axis is connected to a set of pulleys (diameter ratio of 1/20) associated with an electrical motor (Electro-Craft Servo Products, model M1030) that operates with a constant voltage powered by an external DC power supply (Instrutherm, model FA-3050). The platform producing the oscillating pattern is connected to an eccentric wheel.

The synchronization of the measurements is produced by an external trigger connected to a homemade optic sensor and an oscilloscope (Agilent Technologies, model DSO6104A). The oscillation frequency is controlled by adjusting the applied voltage to the electric motor. The NMR hardware used was a Tecmag Redstone console with a Tomco radiofrequency amplifier (model BT00500-AlphaSA).

All the experiments were performed using the Carr-Purcell-Meiboom-Gill (CPMG) pulse sequence with the following standard parameters: duration of the excitation and inversion pulses of 10 μs and 20 μs, respectively, echo time of 400 μs, 12,000 sampled echoes, repetition time of 6 s, and 16 averages. On the other hand, an explicit mention is made when any of these parameters has been changed.

The sample used in these ^{1}H experiments was a 2% (w/v) Sodium-Fluorine Gel (Flugel - DFL) with a neutral pH of about 6.5, viscosity in the range of 7000–20,000 cP, and relative density in the range of 0.850–1.025 g/cm^3. The choice for this gel was due to its higher viscosity compared to distilled water, which avoids turbulent motions during the ^{1}H NMR experiments.

2.2. Mechanically oscillating sample under magnetic field gradients: MOS-NMR

The MOS-NMR experiments are carried out with the sample localized in a region where the magnetic field is given by $B = B_0 + (G{\cdot}r)$, where B_0 is the main magnetic field at the center of the sample, G is the magnetic field gradient across the sample region and r is a particular nuclear spin position.

Considering that the sample oscillates in time along the z direction, then the Larmor frequencies will be given by

$$\omega(t) = \gamma(B_0 + Gz(t)) \tag{1}$$

and the accumulated phase over a period of time by

$$\phi = \int_{t_1}^{t_2} \omega(t)dt = \int_{t_1}^{t_2} \gamma(B_0 + Gz(t))dt \tag{2}$$

Taking into account that the experiments are carried out in the rotating coordinate system, with frequency γB_0, the effective accumulated phase can be written simply by

$$\phi = \int_{t_1}^{t_2} \gamma Gz(t)dt \tag{3}$$

Now, considering that the spin is under a sinusoidal oscillation along the $\hat{z}$-direction, the same direction of the magnetic field gradient G, with amplitude a_0 and frequency Ω, its position $z(t)$ can be written as

$$z(t) = z_0 + a_0 \sin(\Omega t + \theta) \tag{4}$$

where θ is a phase that depends on the initial position of the spin.

In the case of a CPMG MOS-NMR experiment (Fig. 2) as the spin is under a sinusoidal motion along the magnetic field gradient, additional accumulated phases should appear for each dephasing (ϕ_1) and refocusing (ϕ_2) periods τ, around the π pulses, affecting the amplitudes of

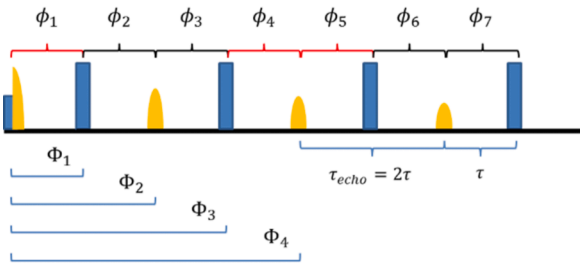

Fig. 2. Visualization of the accumulated phase due to the oscillating motion. The phase Φ of every odd (even) echo will be the combination of every phase ϕ before it, adding the ones marked by black (red) and subtracting the ones marked with red (black).

the observed echoes every instant $\tau_{echo_n} = 2n\tau$.

This effect can be generalized considering the interval of formation of any echo in the CPMG pulse sequence. For this, the general phase between an interval $(n-1)\tau$ and $n\tau$ is given by:

$$\phi_n = \gamma G_0 \int_{(n-1)\tau}^{n\tau} [z_0 + a_0 \sin(\Omega t + \theta)]dt$$
$$= \gamma G_0 z_0 \tau + \frac{\gamma G_0 a_0}{\Omega}[\cos(\Omega(n-1)\tau + \theta) - \cos(\Omega n\tau + \theta)] + b \quad (5)$$

where n is [1, 2, 3, …] and, b is a constant determined by the initial condition $M(0) = M_0$. Every echo has an accumulated phase, Φ, corresponding to the sum of the phases leading up to it, considering the sign changes introduced by the π pulses. Hence, the total accumulated phase is given by:

$$\Phi_n = \phi_n - \Phi_{n-1}(-1)^n, \quad (6)$$

where the term $(-1)^n$ accounts for the effect of the π pulse every 2τ intervals. Echoes occur for every even n. Thus, the NMR signal can be calculated using the following expression:

$$\overline{M}(2j\tau) = M(2j\tau)\exp(-i\Phi_{2j}), \quad (7)$$

where, $\overline{M}$ is the modulated signal caused by the sinusoidal motion of the sample relative to the magnet, τ is the time between the $\pi/2$ and the first π pulse, j is the echo number and Φ_{2j} is given by Eq. (4).

2.3. Spatial selective RF pulse

For NMR experiments performed in the presence of magnetic field gradients, the spectral composition of the RF pulses, defined here with a bandwidth of $\delta\nu$, plays an essential role in the extent of Larmor frequencies that it can resonate. Considering L is the maximum length of the sample along the direction of gradient G, the NMR experiment will be carried out with a Larmor frequency bandwidth given by

$$\Delta\nu = \gamma GL \quad (8)$$

If $\delta\nu < \Delta\nu$, spatial selective excitation will occur, resulting in the excitation of a section perpendicular to the direction of the magnetic field gradient with width $\delta L = \delta\nu/\gamma G$, Fig. 3. In the case of a rectangular RF pulse, the spectral composition is described by a Sinc function [18]. Thus, considering a rectangular RF pulse with a width t_p, the most intense peak of the Sinc function is centered in the interval $\left[-\frac{1}{t_p}, +\frac{1}{t_p}\right]$, which defines the RF excitation predominant bandwidth. For example, considering a rectangular RF pulse of 20 μs, the excitation bandwidth is about 100 kHz. If this RF pulse is applied while under a magnetic field gradient of 35.7 Gauss/cm, a plane with a thickness of approximately 6.7 mm will be selected.

For the CPMG MOS-NMR experiments performed in the presence of magnetic field gradients, the spatial selectivity of the RF pulses results in another significant effect. The region where the RF pulses are effective is the one that is selected by the first excitation pulse (Fig. 3a). However, as the sample sinusoidally moves along the z-direction, part of the initially excited region (selected section) leaves the region where the RF pulses are effective (Fig. 3b), so that the inversion pulses are no longer efficient in producing the CPMG expected echoes, which results in a signal loss proportional to the ratio $\delta l/\Delta L$.

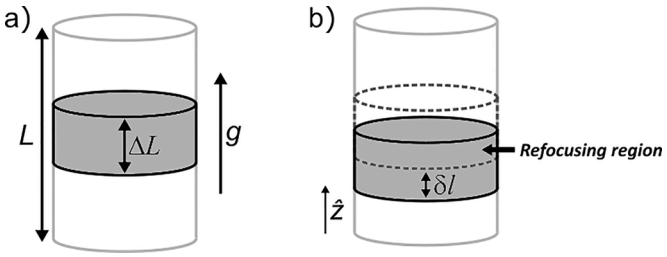

Fig. 3. a) Representation of the NMR sensitive region (ΔL) excited by the first RF pulse in the presence of the magnetic field gradient. b) As the sample moves, the presence of the initially excited spins in the NMR sensitive region becomes smaller than it would be in the case of the static sample, resulting in a signal loss proportional to the ratio $\delta_l/\Delta L$.

3. Results and discussion

As previously described, the experimental apparatus was constructed to control the frequency, amplitude, and sample position relatively to the tool (magnet). Here, the system is more straightforward than what is found in reservoir conditions, both in terms of coil and magnet geometry. Using the solenoid coil is convenient for observing the phase modulation due to the sample movement. Another advantage is the pulse selectivity, which becomes less complex on the solenoid as the applied RF magnetic field is quite uniform in the sweet spot.

Fig. 4 shows the signal decay observed by CPMG pulse sequence (Fig. 4a) and the respective T_2 distribution for the ^{1}H Flugel experiment with the sample static (Fig. 4b), for reference.

3.1. CPMG-MOS-NMR decay

To explore the phase modulation effects and analyze them from the theoretical and operational point of views, most of the experiments were performed with an echo time of 400 μs, which lowers the contribution from the diffusion effect. To analyze the effects of diffusion, CPMG-MOS experiments were run with longer echo times of 600 μs, 800 μs, 1000 μs and 1200 μs.

One of the differences between the signal in uniform magnetic fields and the signal in high gradients is the narrowing of the observed echo. In the case of a uniform magnetic field, the echo might be broad enough to be observable over a range longer than milliseconds. Therefore, the region around its center is flat enough that acquiring more points before and after the exact CPMG refocusing time can increase the signal to noise ratio without affecting the average intensity value. The same cannot be carried out in a system with high gradients due to the echo narrowing, where the points around the echo center quickly decay, and tens of microseconds to either side will go through a significant change in magnitude and phase. The disadvantage in this case is the lower signal-to-noise ratio obtained.

Fig. 5 shows the echo profile obtained by summing the first 1000 echoes for the Flugel sample, which increases the signal-to-noise ratio and allows for an easier determination of the central echo position.

In the case where the sample is in motion, the phase modulation effects are strongly affected by the window in which the echo is observed. In general, the theory describes the observed effects considering the maximum of refocusing, that is, the echo center. Therefore, as

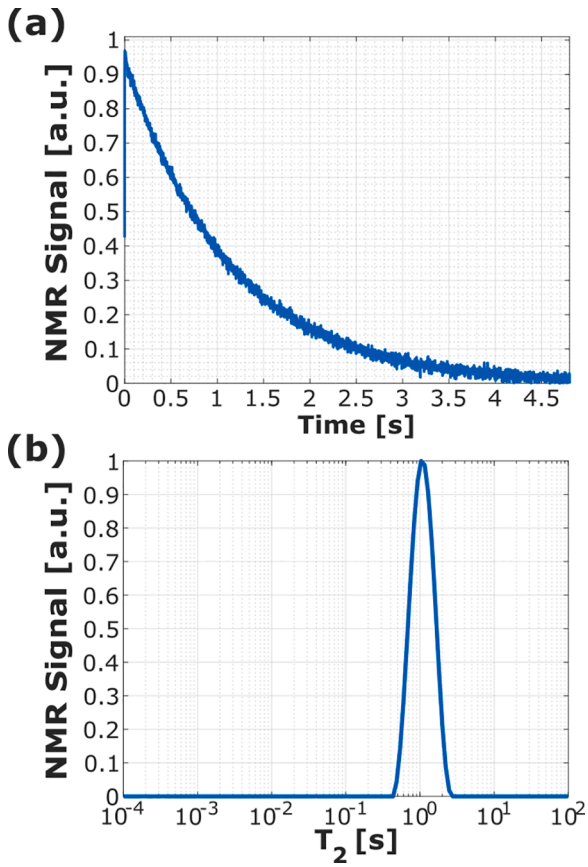

Fig. 4. (a) ^{1}H Measured decay observed from CPMG pulse sequence for a bulk sample of Flugel and (b) respective distribution of relaxation times.

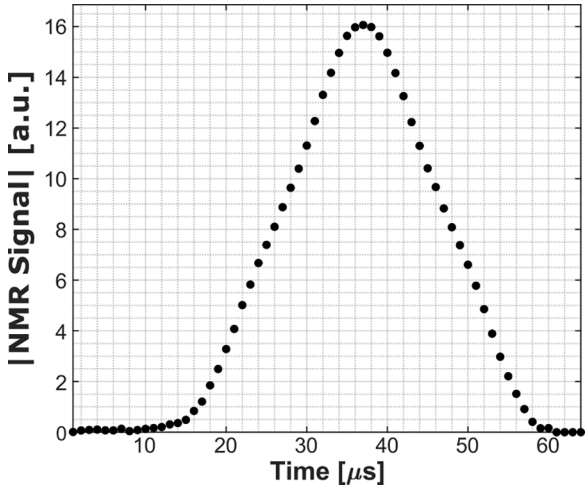

Fig. 5. Echo shape obtained by the sum of the first thousand echoes of a CPMG pulse sequence. Considering the increased signal-to-noise ratio, it is easier to determine which points in the acquisition window could be considered to determine the echo intensity.

described by Coman et al. [10], the effects of phase modulation are expected to be smaller than 10% in most cases.

Fig. 6 shows the results of different windows of observation: 1, 17 and 64 points with a dwell time of 1 μs. It can be observed that despite the gain in the signal-to-noise ratio, the signal becomes strongly modulated with the larger observation window. The theory predicts the behavior of the signal at maximum echo refocusing, where minimum modulation is expected as observed. Regions other than the maximum will also have a strong influence on the position of the nuclei given the strong magnetic field gradient. Therefore, using the smallest observation window yields results closer to those predicted in the theory presented above, but with a considerably lower signal-to-noise ratio.

Although the signal modulation is stronger when a larger echo window is considered, these data can be used both to indicate where the sample movement is present, as well as to identify the frequency spectrum of the oscillation.

Fig. 7 shows the frequency spectrum computed for the three different windows of observation that were presented in Fig. 6. The spectrum was calculated by the Fourier transform of the difference between the signal and the adjustment obtained by the Laplace transform of the signal, which minimizes the contributions from the exponential decays. Some components can be observed in multiples of 4 Hz, which was the oscillation frequency of the setup for this experiment, and the modulation lines are clearer in the case of a larger observation window.

In addition to the phase modulation, the time evolution of magnetization is strongly influenced by the selectivity of the RF pulse. This effect appears at the beginning of the signal. Fig. 6 shows the result for an oscillation with a frequency of 4 Hz and an amplitude of 2 mm, where this effect is easily observed. Thus, the signal can be separated into two regions. The first, where the two effects occur simultaneously, which manifests itself until the magnetization present in the sensitive region of NMR reaches a steady state with amplitude proportional to (1 - δl/ΔL), after a time interval of the order of a period of oscillation of the sample. After this transient period, magnetization evolves only under the effect of phase modulation.

3.2. *Spatial selectivity and synchronization behavior*

An important point that was observed from Eq. (4) is the dependence of the signal modulation patterns on the initial sample position. To evaluate this dependence, a synchronization system was coupled to the experimental setup. Therefore, setting the amplitude and frequency of the oscillation, the magnetization decay was measured for $\theta = 0^{\circ}$ and $\theta = 90^{\circ}$, which defines two different conditions to the initial position described in Eq. (4). In addition to the initial position, it is worth mentioning that the initial velocity is different in the two conditions, in which the maximum for $\theta = 0^{\circ}$ and the minimum for $\theta = 90^{\circ}$

Fig. 8 shows the theoretical and experimental results. It can be observed in this figure, especially in the case for $\theta = 0^{\circ}$, that the modulation seems to double the frequency, which is in agreement with what is observed in Fig. 7 with the Fourier transform.

Fig. 9 shows the results for a fixed frequency, 2 Hz, and different amplitudes of 0.5, 1.0, 1.5, and 2.0 mm. The decay was computed considering the echo center, and the relaxation times distribution was obtained. Two different relaxation times are observed for all cases, and the intensity of each contribution depends on the amplitude of oscillation. It can be observed that there are two components of relaxation, where the fastest decay has a duration of ~0.25 s, which is half of the oscillation period. Therefore, considering that this was a synchronized experiment, where the sample started from the maximum amplitude, and during half of the oscillation period the magnetization was being displaced from the initially excited region, it can be concluded that the fast component is due to the spatial selectivity of the RF pulse.

Fig. 10 shows the intensity of the shorter T_2, originating from the RF pulse selectivity, increasing with the amplitude of oscillation. The observed quasi-linear relationship is related to the excitation profile, and therefore, for different conditions, such as another type of coil and gradient magnetic field, the relationship might not be linear.

The relaxation time for each peak was constant for different amplitudes and a fixed frequency, with a variation only in the signal amplitude. However, since the shorter T_2 is associated with the oscillation period, the relaxation time for the shorter relaxation peak will change with the frequency. Fig. 11 shows the relaxation time distribution for the

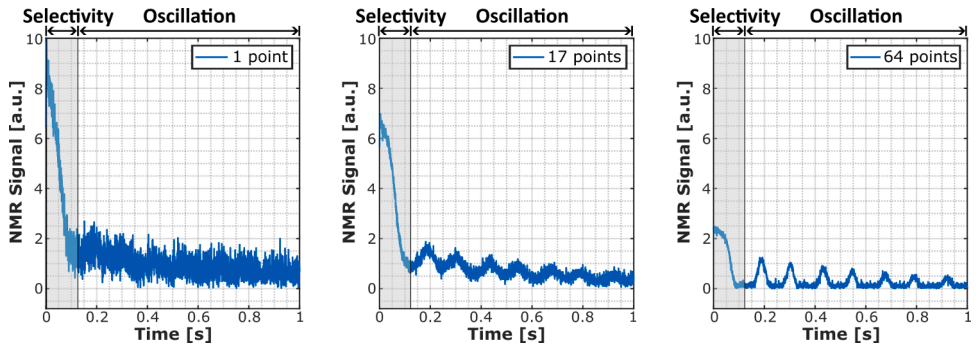

Fig. 6. Post-processing of CPMG data with different number of points per echo. Out of the 64 data points acquired per echo, the graph on the left shows the signal when considering only the central point of the echo; the middle graph shows the signal when using the central point plus 8 points before and 8 points after the center; and the graph on the right shows the signal when using all the 64-points in the echo window. The oscillation was with an amplitude of 2 mm and a frequency of 4 Hz.

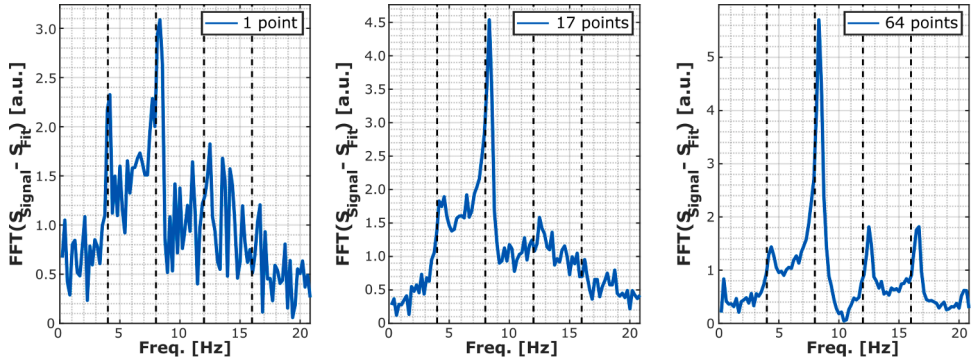

Fig. 7. Fourier Transform of the data obtained from the difference between the NMR data and the fitting calculated from the Inverse Laplace transformation algorithm for each decay shown in Fig. 6.

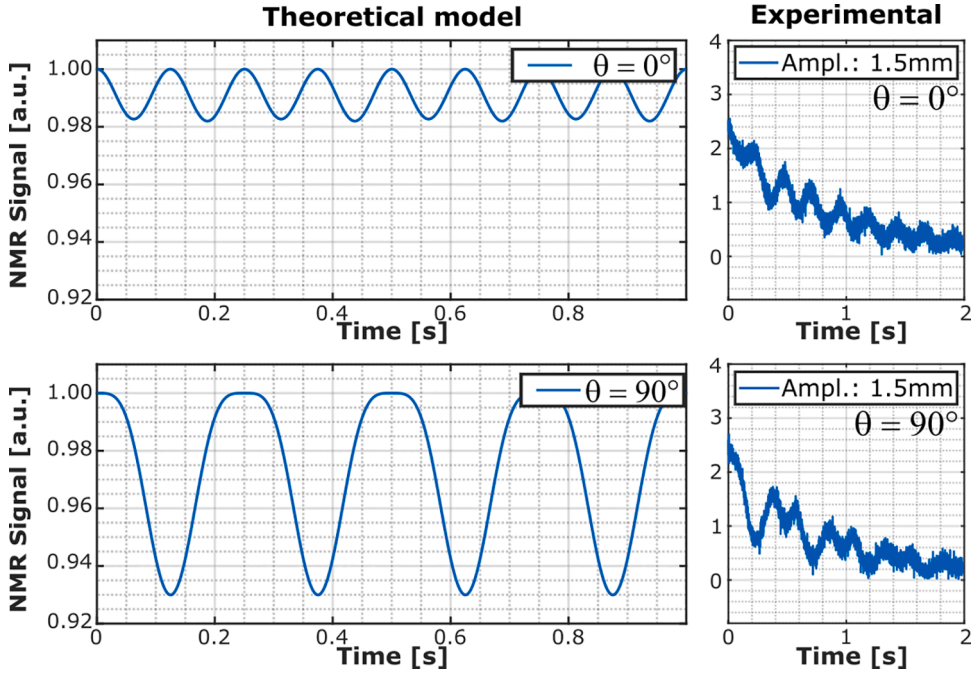

Fig. 8. Comparison between experimental data obtained from CPMG pulse sequences and those acquired from modulation curves predicted by the theoretical model. Curves were obtained for the conditions of $\theta = 0^{\circ}$ and $\theta = 90^{\circ}$, which have different beating patterns.

cases where the amplitude is constant, 2.0 mm, and the frequencies vary: 1, 2 and 4 Hz. The increase in the relaxation rate due to the selective pulse is observed both in the decay curve and in the relaxation time distribution.

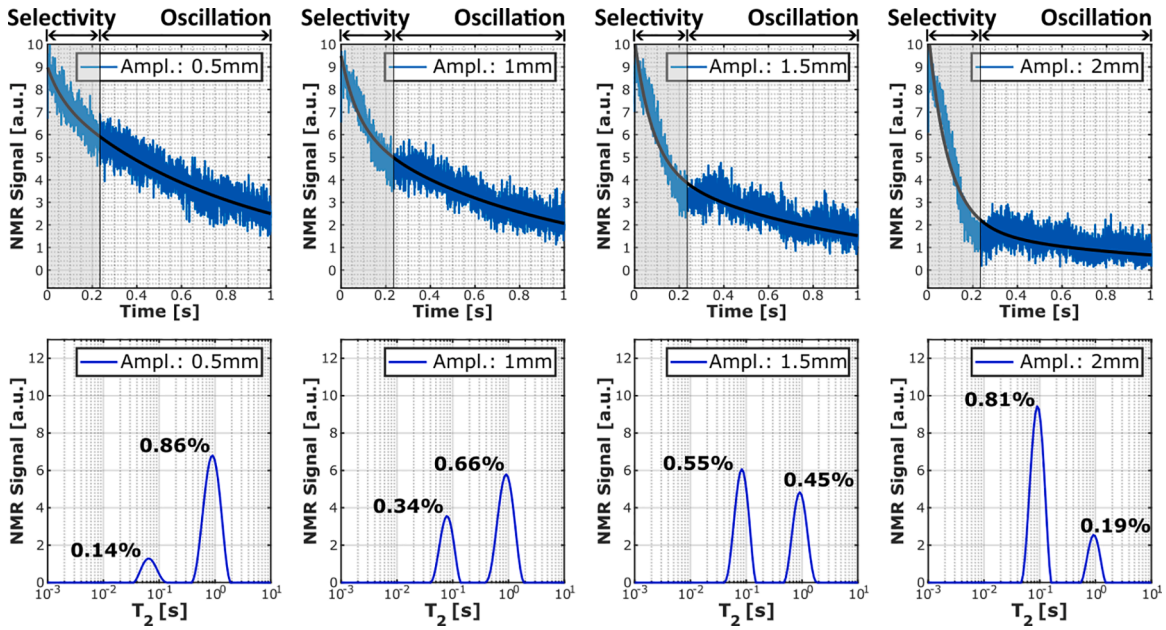

Fig. 9. Each column shows the observed NMR signal for different oscillation amplitudes and its respective Inverse Laplace Transform. Note that the $T_{2,Selec}$, related to the period of the oscillatory motion, appears to be constant through different oscillation amplitudes, while its contribution increases together with the increase in oscillation amplitude.

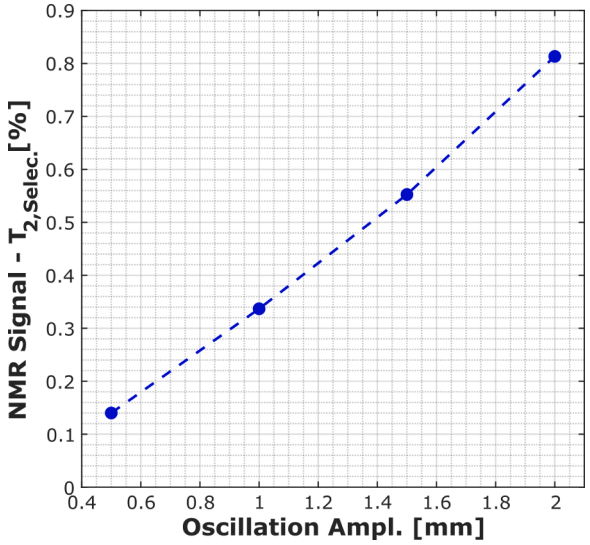

Fig. 10. Intensity of the shorter relaxation time peak as a function of tool oscillation amplitude for the frequency oscillation of 2 Hz. There is a mostly linear correlation between oscillation amplitude and the contribution of the shorter relaxation time to NMR data.

3.3. MOS-NMR and echo time effects

Another parameter in the pulse sequence that has a large impact on the NMR signal is the value of the echo time. The echo time represents the time delay from the center of the radio frequency pulse to the center of the echo signal.

Fig. 12 below shows the behavior of the NMR signal in an LWD simulation experiment at a fixed oscillation amplitude of 2.0 mm, as a function of echo time and oscillation frequency. When the sample is not oscillating, we see shorter decays for longer echo times. This is because of spin coherence loss due to the translational diffusion in the presence of the magnetic field gradient. This decay will be even shorter when the sample is mechanically oscillating due to both effects.

As commented before, the initial signal loss in times shorter than an oscillation period is related to the flow effect (as described by Coman et al. [10]) of moving the volume initially selected by the 90° pulse to regions of slightly different frequencies. This means regions in which the refocusing pulses are less effective and in which the sensor is less sensitive. This results in an effective smaller region of excited sample contributing to the observed signal.

4. Conclusions

Understanding the effects of mechanical oscillations during LWD measurements is extremely helpful in improving the predictions made from this type of well logging. Thus, having a controlled environment in which one can control specific motions relative to the magnetic field can lead to describing the origin of specific observed patterns in the complex NMR signal observed.

In the case of our LWD simulator, the effects associated with the selectivity of the RF pulses from the phase modulation can be clearly distinguished, obtaining the correct T_2 values of the studied liquids.

Although the Fast Fourier Transform (FFT) can identify some oscillatory components associated with sample movement, we are currently considering different techniques to analyze our complex temporal signals with low signal-to-noise ratio, not limited to FFT. However, for the data presented in the manuscript, even using only ILT, we were able to separate the decays due to the transverse relaxation of the operational effects associated with the oscillatory movement of the samples.

Finally, this work presents experimental results obtained with our LWD simulator that were well understood and explained through the basic theoretical method used. As an evolution perspective for this work, we are selecting a set of representative rocks of the sandstone and carbonate families to be studied with the equipment presented in this manuscript. In order to minimize the effects associated with RF pulse selectivity, more efficient probes must be designed to allow the application of shorter RF pulses.

Declaration of Competing Interest

The authors declare that they have no known competing financial interests or personal relationships that could have appeared to influence

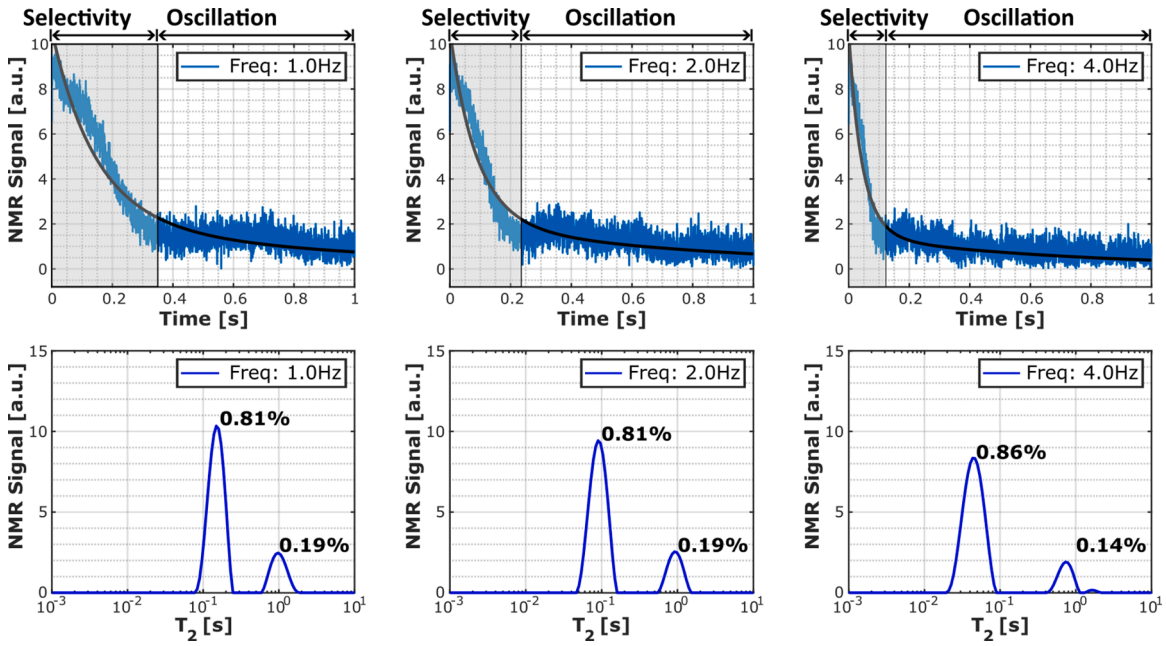

Fig. 11. NMR data and its respective Inverse Laplace Transform in an experiment with 2.0 mm of oscillation amplitude as a function of different oscillation frequencies. Note that the short relaxation time component moves to shorter values as the frequency increases, but its amplitude remains practically constant.

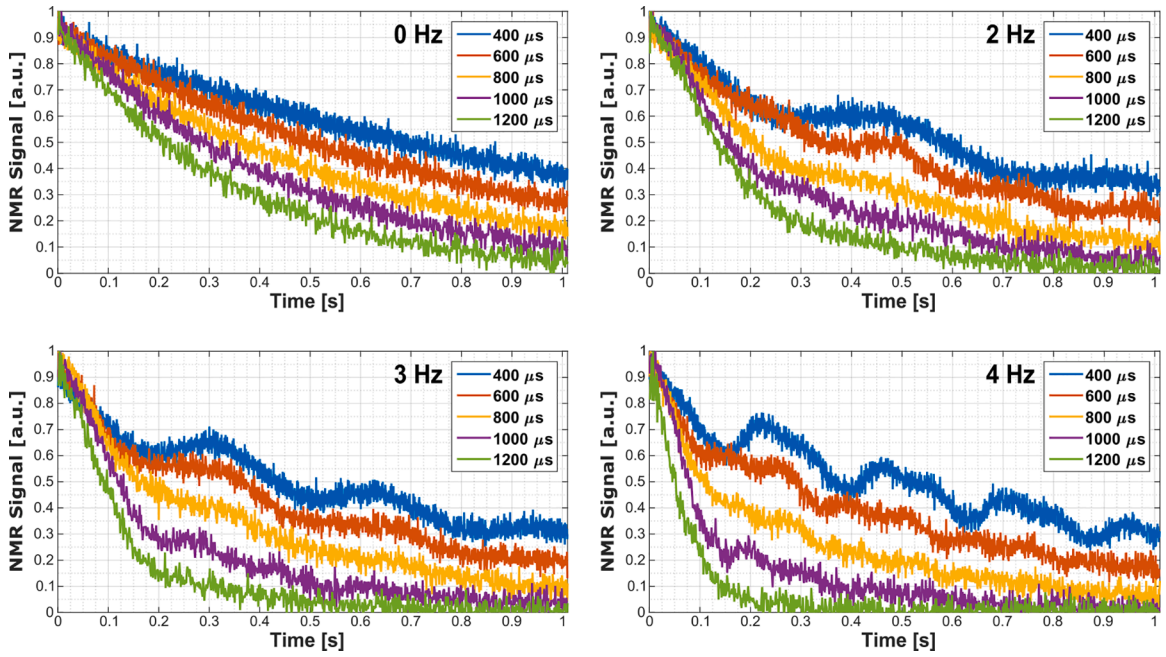

Fig. 12. The behavior of NMR data as a function of oscillation frequency (different graphs) and echo time (different colors in the same graph) at a fixed oscillation amplitude of 2.0 mm. The additional signal loss in 2, 3, and 4 Hz oscillation frequency is related to the flow effect across the sensitive volume.

the work reported in this paper.

Data availability

Data will be made available on request.

Acknowledgements

Authors acknowledge the support of the following Brazilian Institutions: University of São Paulo (USP) and Centro de Pesquisa e Desenvolvimento Leopoldo Américo Miguez de Mello (CENPES/Petrobras, 2020/00010-0). T. J. Bonagamba acknowledges the National Council for Scientific and Technological Development, Brazil (CNPq, 308076/2018-4) and the São Paulo Research Foundation, Brazil (FAPESP, 2009/54880-6).

References

[1] C.P. Slichter, Principles of Magnetic Resonance, Springer Berlin Heidelberg, Berlin, Heidelberg, 1990, https://doi.org/10.1007/978-3-662-09441-9.
[2] L.F. Montes, E.C.S. Oliveira, Á.C. Neto, S.M.C. Menezes, E.R.V. Castro, L.L. Barbosa, Low-field NMR: a new alternative to determine the aromatic content of petroleum

distillates, Fuel 239 (2019) 413–420, https://doi.org/10.1016/J.FUEL.2018.11.024.
[3] R.L. Kleinberg, J.A. Jackson, An introduction to the history of NMR well logging, Concepts Magn. Reson. 13 (2001) 340–342, https://doi.org/10.1002/CMR.1018.
[4] E. Lucas-Oliveira, A.G. Araújo-Ferreira, T.J. Bonagamba, Surface relaxivity probed by short-diffusion time NMR and Digital Rock NMR simulation, J.Petrol. Sci. Eng. 207 (2021), https://doi.org/10.1016/j.petrol.2021.109078.
[5] M.H. Jácomo, R.I.F. Trindade, E. Lucas-Oliveira, T.J. Bonagamba, Magnetic matrix effects on NMR relaxation times in sandstones: a case study in Solimões Basin, J. Appl. Geophy. 179 (2020), https://doi.org/10.1016/j.jappgeo.2020.104081.
[6] M.H. Jácomo, R.I.F. Trindade, M. French, E. Lucas-Oliveira, E.T. Montrazi, T. J. Bonagamba, Nuclear magnetic resonance characterization of porosity-preserving microcrystalline quartz coatings in Fontainebleau sandstones, Am. Assoc. Pet. Geol. Bull. 103 (2019) 2117–2137, https://doi.org/10.1306/01301918104.
[7] K.-J. Dunn, D.J. Bergman, G.A. Latorraca, Nuclear Magnetic resonance: Petrophysical and Logging Applications, Pergamon, San Ramon, 2002.
[8] M.G.P. George R. Coates, Lizhi Xiao, NMR logging: Principles and Applications, Houston, 1999. https://www.halliburton.com/content/dam/ps/public/lp/contents/Books_and_Catalogs/web/NMR-Logging-Principles-and-Applications.pdf (accessed December 5, 2019).
[9] M.G. Prammer, NMR logging-while-drilling (1995-2000), Concepts Magn. Reson. 13 (2001) 409–411, https://doi.org/10.1002/CMR.1029.
[10] R. Coman, H. Thern, T. Kischkat, Lateral-motion correction of NMR logging-while-drilling data, in: SPWLA 59th Annual Logging Symposium, 2018.
[11] K.T. O'Neill, T.A.J. Hopper, E.O. Fridjonsson, M.L. Johns, Quantifying motional dynamics in nuclear magnetic resonance logging, J. Magn. Reson. 337 (2022), https://doi.org/10.1016/J.JMR.2022.107167.
[12] W. Selby, P. Garland, I. Mastikhin, Dynamic mechanical analysis with portable NMR, J. Magn. Reson. 339 (2022), https://doi.org/10.1016/J.JMR.2022.107211.
[13] R.L. Kleinberg, NMR measurement of petrophysical properties, Concepts Magn. Reson. 13 (2001) 404–406, https://doi.org/10.1002/CMR.1027.
[14] M.G. Prammer, Hydrocarbon saturation measurements by NMR, Concepts Magn. Reson. 13 (2001) 406–408, https://doi.org/10.1002/CMR.1028.
[15] R. de Oliveira-Silva, É. Lucas-Oliveira, A.G. de Araújo-Ferreira, W.A. Trevizan, E.L. G. Vidoto, D. Sakellariou, T.J. Bonagamba, A benchtop single-sided magnet with NMR well-logging tool specifications – examples of application, J. Magn. Reson. 322 (2021), 106871, https://doi.org/10.1016/j.jmr.2020.106871.
[16] B. Blümich, P. Blümler, G. Eidmann, A. Guthausen, R. Haken, U. Schmitz, K. Saito, G. Zimmer, The NMR-MOUSE: construction, excitation, and applications, Magn. Reson. Imaging (1998) 479–484, https://doi.org/10.1016/S0730-725X(98)000691.
[17] Eiichi. Fukushima, S.B.W. Roeder, Experimental Pulse NMR: a Nuts and Bolts Approach, Addison-Wesley Pub. Co., Advanced Book Program, 1981.
[18] E.O. Brigham, The fast fourier transform and its applications by E. Oran Brigham, Education IEEE Transactions On 12 (1988), 448.